STRUCTURAL PARAMETERS OPTIMIZATION AND EXPERIMENT OF TRENCHING BLADES VIA DEM

/

基于 DEM 的开沟刀结构参数优化与试验

Haochao TAN, Congcong SHEN, Zhaoyang GUO, Deyu LI, Shuai MA, Liming XU *) [1]
College of Engineering, China Agricultural University, Beijing 100083/China
Corresponding author: Liming XU
Tel: +86 010-62737291; E-mail: xulimingcoe@cau.edu.cn
DOI: https://doi.org/10.35633/inmateh-74-82

Keywords: *trenching blades; structural parameter optimization; DEM; experimentation*

ABSTRACT

This study developed a chain counter-rotating trenching and backfilling device to reduce high tillage resistance in orchard operations. A 3D mathematical model of the trenching blade was created using Cartesian coordinate transformation. Taking curvature (β), curve angle (α), bend radius (R), and cone residual angle (θ) as experimental factors, and soil cutting resistance as the evaluation index. The optimized parameters were β=95°, α=10°, R=24 mm, θ=39°. Bench tests were performed with the optimal parameters, and the results showed that the optimized ditching blade reduced the resistance by 18.7% compared to the ordinary trenching blades. Field test results showed a 9.64% reduction in furrowing torque.

摘要

针对果园开沟过程中耕作阻力大的问题，本文提出了一种链条反向旋转开沟回填装置。通过笛卡尔坐标系变换，建立开沟刀的三维数学描述模型。以曲率(β)，曲线角度(α)，弯折半径(R)和锥余角(θ)为试验因素，以切土阻力为评价指标进行试验，优化后的参数为 β=95°，α=10°，R=24 mm，θ=39°。以最优参数进行台架和田间试验，台架试验表明，相对于普通开沟刀，优化后的开沟刀阻力减少了 18.7%，田间试验表明，相对于普通开沟刀，装配有 BS 刀的开沟扭矩降低了 9.64%。

INTRODUCTION

Tillage has been a long-standing practice in agricultural production (*Sadek et al., 2021*), and the continuous improvement of tillage techniques has been a key focus in the agricultural industry *(Green et al., 2023*). The use of agricultural machinery in the tillage process has significantly enhanced operational efficiency, reduced manual labor, lowered costs, and improved the overall quality of agricultural production *(Li et al., 2023; Wang, Zhou et al, 2024*). Trenching and fertilization are an important part of crop growth. For deep-rooted crops such as grapes, the trench depth is generally deeper, often requiring 60 cm. Disc-type trenching equipment struggles to achieve such depths, making chain-type trenching devices a good choice for agricultural deep trenching.

The trenching blade is a key operating component in chain-type trenching devices, and studying the interaction between the tool and the soil is crucial for optimizing and improving its performance. Reasonably designed parameters can significantly enhance operation efficiency, reduce operational resistance, minimize trenching torque, and promote sustainable agricultural development (*Liu, et al., 2023; Wang, Zhang et al, 2024; Wei et al., 2024)*. Reducing the tillage resistance agricultural components has always been the goal pursued by agricultural experts. *Hu Zhiyong et al., (2017),* conducted a structural statics, dynamic modal, and harmonic response analysis of a variant form of trenching blades using finite element analysis. The results showed that the trenching blades would not experience body forging and distortion during operation. *Wang Xu, et al., (2023)*, analyzed the force exerted on trenching blades during trenching, straw burial, and soil backfilling processes using a chain trenching device but did not optimize the structure parameters of the trenching blades. *Kim et al., (2019),* applied a chain trenching device underwater and employed genetic algorithms for multi-objective optimization of the trenching machine, aiming to minimize power and weight during operation. *Sitorus et al., (2016),* developed a kinematic and dynamic analysis model and designed a chain trenching machine for underwater applications.

[1] *Haochao Tan, Ph.D.; Congcong Shen, Ph.D.; Zhaoyang Guo, Ph.D.; Deyu Li, Ms.; Shuai Ma, Associate professor Ph.D.; Liming Xu, Professor, Ph.D.*

They analyzed the effects of cutting tools, material conditions, working parameters, and structural parameters on forces, torques, weight, and power components. *Azimi-Nejadian et al., (2022),* used the DEM to study the influence of plow design parameters, plow depth, and operating speed on the burial depth of weed seeds. *Zhang et al., (2022),* used the DEM to establish an interaction model between soil and rotary tiller roller, analyzed the dynamic process of soil cutting by the rotary tiller blade, and obtained the changes in soil deformation area, cutting energy, cutting resistance, and soil particle movement. *Ma et al., (2024),* designed a double-disk trencher, utilized a 3D scanner to scan the trenching blade, established a 3D model of the trenching blade, and analyzed stress and strain conditions. The results showed that the maximum stress was 55.48 MPa, and the average deformation was 0.38 mm, meeting the usage requirements of the trenching blade. *Song et al., (2022),* established a furrow opener model using 3D software. Through simulation experiments, they compared and analyzed the soil disturbance behavior of the furrow opener under different positions, speeds, and working depths. The results showed that the relative errors of the cross-sectional area for the front and rear furrow openers were 0.25% and 5.2%, respectively. The simulation results accurately reflected the soil disturbance during the furrowing process. Zeng et al., (2024), have designed a standard ditching blade with a self-excited vibration device. A simulation model of soil and the ditching blade was established and experiments were conducted. The results show that compared to common ditching device, the self-excited vibration device reduces resistance by 12.3%. *Song et al., (2024),* designed a trenching blade that combines cutting and throwing actions. Through simulations, the main factors affecting trenching performance were identified, the trenching blade was fabricated, and the tests were conducted. The results show that the trenching power consumption is 0.668 kW, and the soil fragmentation rate is 92.4%, meeting the quality requirements for trenching.

The aforementioned scholars have investigated the relationships between different soil-engaging components and the soil, reducing overall furrowing resistance, which holds significant research importance. However, there is still a lack of precise in-depth analysis concerning the trenching blades used in chain-type trenching devices, necessitating an analysis and optimization of the structural characteristics of the trenching blades. In response to the above issue, this study aims to establish a mathematical description model of the trenching blades, systematically design and optimize the structural parameters of the trenching blades, and manufacture new trenching blades (hereinafter referred to as BS blades) based on the optimal parameters. Subsequently, the practical effects of BS blades in reducing soil cutting resistance and torque will be verified through field trials, providing theoretical and technical support for achieving efficient and energy-saving furrowing operations.

MATERIAL AND METHODS

Structure and working principle

This article proposes a novel chain reverse rotation trenching device to meet the requirements of trenching, fertilizing, and backfilling. The overall structure is shown in Fig.1a. It mainly consists of a frame, ground wheel, hydraulic cylinder, and trenching blade (Material is 65Mn). The trenching depth is adjustable by extending the hydraulic cylinder, and the trenching blade is fixed in reverse with the blade edge facing downward, to achieve downward cutting of the soil. During this process, the trenching blade is an important component in the operation.

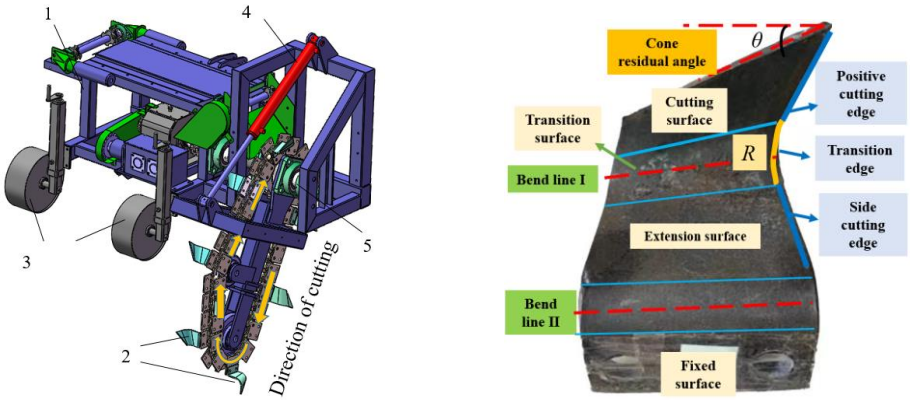

a) Entire schematic diagram of the machine *b) Schematic diagram of trenching blade structure*

Fig. 1- Trenching machine structure

1-Frame; 2-Trenching blade; 3- Ground wheel; 4-Hydraulic cylinder; 5-Drive shaft

Fig.1b is a structural diagram of the ditching blade, which includes the cutting surface, transition surface, extension surface, fixation surface, side cutting edge, transition edge, and positive cutting edge. Among them, the positive cutting edge directly participates in cutting the soil, while the side cutting edge has almost no cutting effect. The transition edge is in an arc shape, realizing the transition from the positive cutting edge to the side cutting edge. The cutting surface, where the positive cutting edge is positioned, serves as the primary cutting role. The cone residual angle (θ) is an important parameter affecting the size of the cutting area. The transition surface is a curved surface, achieving the transition from the cutting surface to the extension surface. It participates in a small part of the cutting. The size of bend radius(R) affects the area of the cutting surface and the transition surface. The extension surface does not participate in cutting and its main function is to extend the cutting surface outward to achieve different trench widths. Based on the length of the extension surface, the ditching blades can be classified into models of 12, 15, 20, 25, and 30 cm. Different models of ditching blades only differ in the length of the extension surface; the cutting surface parts are exactly the same.

Analysis of trenching blades structure parameters

To facilitate the analysis of the formation process of the trenching blade, a right-handed coordinate system X'''Y'''Z''' was established (Fig.2a), the X'''-axis coincides with the bending line *I* and points towards the positive cutting edge. The Y'''-axis coincides with the cutting surface and is perpendicular to the direction of bending line *I*. The Z'''-axis is perpendicular to the cutting surface and points towards the fixation surface. In this coordinate system, rotate it β degrees in the negative direction of the X''' axis to obtain the coordinate system X''Y''Z'', indicated by a single dashed line. Then, rotate it α degrees in the negative direction of the Z'' axis to obtain the coordinate system X'Y'Z', indicated by a double dashed line. At this point, the unfolding diagram of the trenching blade is obtained (Fig. 2b).

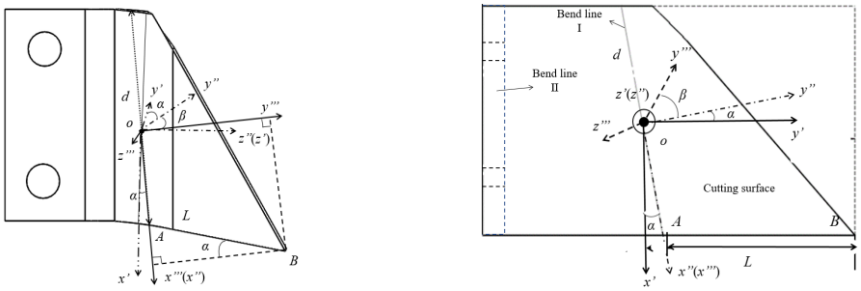

a) Diagram of trenching blade after bending *b) Expanded diagram of trenching blade*

Fig. 2- Bending diagram of trenching blades

Note: A and B represent the two endpoints of the cutting edge; d represents the length of bend line I, mm; L represents the distance between A and B points, mm; α represents the inclination angle of bend line I, (°); β represents the bending angle of the cutting surface, (°).

In the X'''Y'''Z''' coordinate system, the position of the positive cutting edge can be described by its two endpoints, *A* and *B*. We can solve for the coordinates of the two endpoints *A* and *B* using Equation(1):

$$A=\begin{pmatrix}\frac{d}{2}\\0\\0\end{pmatrix} B=\begin{pmatrix}\frac{d}{2}+L\sin\alpha\\L\cos\alpha\\0\end{pmatrix} \quad (1)$$

The equation for the relationship between the coordinates of points *A* and *B* in the X'Y'Z' coordinate system, as shown in Equation (2), can be derived.

$$C=\mathrm{Rot}(Z'',\alpha)\mathrm{Rot}(X''',\beta)i \quad (2)$$

where i is the coordinate value to be converted, and C is the converted coordinate value, specifically expanded as (3):

$$\begin{pmatrix}x'\\y'\\z'\end{pmatrix}=\begin{pmatrix}\cos\alpha&-\sin\alpha&0\\\sin\alpha&\cos\alpha&0\\0&0&1\end{pmatrix}\begin{pmatrix}1&0&0\\0&\cos\beta&-\sin\beta\\0&\sin\beta&\cos\beta\end{pmatrix}\begin{pmatrix}x'''\\y'''\\z'''\end{pmatrix} \quad (3)$$

where x', y', z' and x''', y''', z''' are the coordinates of points *A* and *B* in the coordinate systems X'Y'Z' and X'''Y'''Z''' respectively.

Solving equations 1 and 3, the coordinates of points *A* and *B* on positive cutting edges are obtained, respectively:

$$A=\begin{pmatrix}\frac{d}{2}\cos\alpha\\ \frac{d}{2}\sin\alpha\\ 0\end{pmatrix}\quad B=\begin{pmatrix}\cos\alpha(\frac{d}{2}+L\sin\alpha)-L\cos^2\alpha\sin\alpha\\ \sin\alpha(\frac{d}{2}+L\sin\alpha)+L\cos^3\alpha\\ L\cos\alpha\sin\alpha\end{pmatrix} \tag{4}$$

The position of the positive cutting edge varies, leading to different angles of entry into the soil and consequently different cutting resistances. From equation (4), it can be observed that the factors affecting the variation in the position of the positive cutting edge primarily include the bending line angle α, the curvature β, the length of the positive cutting edge L, and the length of the bending line d. The length of the positive cutting edge is typically around 45 mm, so L can be considered as a constant. According to the Chinese national standard GB/T1243-2006, a 32A chain with a pitch of 50.8 mm is used for chain trenching devices. The parameter d is related to pitch, so the focus can be on the influence of α. Based on the analysis in the two sections above, the factors influencing the trenching blade cutting process include α, β, R, and θ.

Experimental design

By optimizing these parameters, the efficiency and functionality of the trenching blades can be improved. Central Composite Design (CCD) experiments were conducted with α values of 5°, 10°, 15°, 20°, and 25°, β values of 75°, 94°, 112°, 131°, and 150°, R values of 10, 15, 20, 25, and 30, θ values of 0°, 10°, 20°, 30°, and 40° to optimize the parameters of the trenching blade structure. A total of 30 experiments were conducted, including 24 experiments with different combinations of structural parameters and 6 repeated experiments. The cutting resistance (F_1) of the trenching blade fully entering the soil was chosen as the test index. Based on the structural parameters, SolidWorks (2016) was utilized to generate three-dimensional models for 24 distinctively shaped trenching blades intended for the experiment (Fig. 3a exhibits only 12 of them) and preserved them in .step format. Afterward, they were imported into the discrete element simulation software, employing the parameters outlined in Table 2 for the discrete element simulation. Given the reduced space necessary for single-blade soil cutting tests, the trench box dimensions in EDEM were configured to 2000 mm × 400 mm × 600 mm (Fig.3b). To expedite the computation process, the simulation duration was set to 0.5 seconds with a time step of 0.01 seconds.

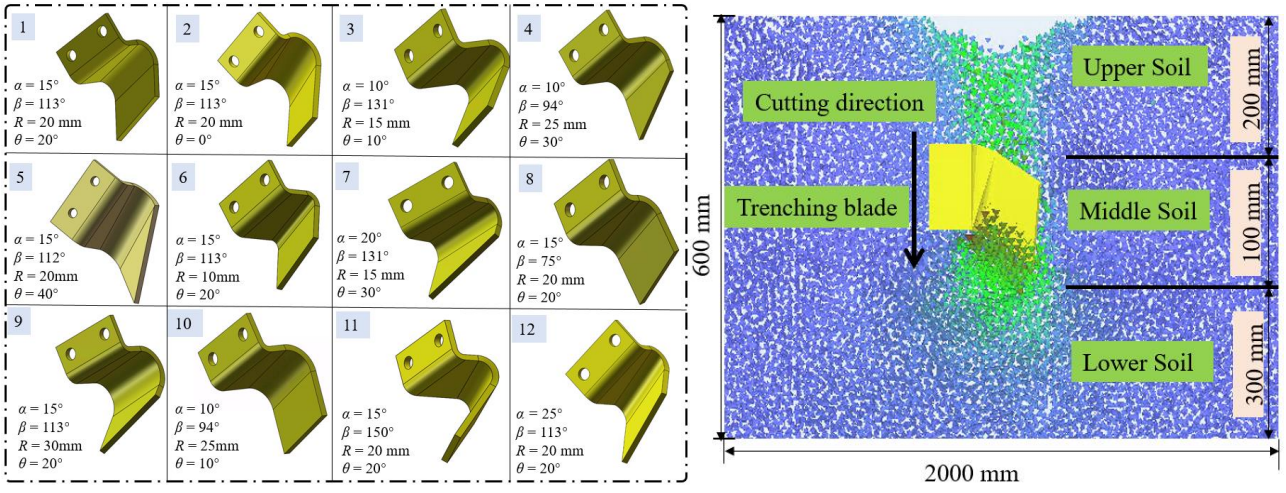

a) Trenching blade with different paraments *b) Simulation model*

Fig. 3 - The models of the trenching blades with different structural parameters

Table 1

The experimental factors and level designs for the Central Composite Design

No.	Actual factor level				Coded factor level				Test indicators
	Curvature β / °	Bending line angle α /°	Bend radius R / mm	Cone residual angle θ / °	Curvature β / °	Bending line angle α / °	Bend radius R / mm	Cone residual angle θ / °	Cutting resistance F_1 / N
0	1	2	3	4	5	6	7	8	9
1	131.25	10	15	30	1	-1	-1	1	648.58
2	131.25	20	25	10	1	1	1	-1	1038.48
3	131.25	20	15	30	1	1	-1	1	739.59
4	75	15	20	20	-2	0	0	0	588.46
5	150	15	20	20	2	0	0	0	799.9

0	1	2	3	4	5	6	7	8	9
6	131.25	10	25	30	1	-1	1	1	690.02
7	112.5	15	30	20	0	0	2	0	881.06
8	93.75	10	25	10	-1	-1	1	-1	688.05
9	93.75	10	15	10	-1	-1	-1	-1	599.48
10	112.5	5	20	20	0	-2	0	0	546.6
11	112.5	15	20	40	0	0	0	2	600.82
12	131.25	20	25	30	1	1	1	1	878.17
13	112.5	15	10	20	0	0	-2	0	664.47
14	112.5	25	20	20	0	2	0	0	1011.97
15	93.75	20	15	30	-1	1	-1	1	666.01
16	93.75	10	25	30	-1	-1	1	1	477.76
17	93.75	20	25	30	-1	1	1	1	783.87
18	131.25	10	15	10	1	-1	-1	-1	689.38
19	131.25	10	25	10	1	-1	1	-1	809.58
20	93.75	20	25	10	-1	1	1	-1	931.76
21	93.75	20	15	10	-1	1	-1	-1	848.69
22	112.5	15	20	0	0	0	0	-2	890.63
23	131.25	20	15	10	1	1	-1	-1	795.3
24	93.75	10	15	30	-1	-1	-1	1	619.99
25	112.5	15	20	20	0	0	0	0	754.56

Table 2

Parameters of discrete element simulation for soil

Type	Static friction coefficient	Rolling friction coefficient	Restitution coefficient	Adhesive energy density / (J m^{-3})
Upper soil	0.6	0.07	0.47	2694
Middle soil	0.5	0.17	0.52	4266
Lower soil	0.5	0.21	0.62	4432
65Mn- Upper soil	0.72	0.33	0.44	-
65Mn- Middle soil	0.8	0.16	0.54	-
65Mn- Lower soil	0.7	0.32	0.51	-

Validation test

The experiment consists of two parts: the first part involves using a universal testing machine to measure the cutting resistance of the trenching blade. The purpose is to compare the cutting resistance of BS blade with that of a conventional one (hereinafter referred to as CS blade). The second part involves the mean trenching torque. During field operations, the trenching process is the result of the combined action of multiple trenching blades. All trenching blades are driven by a drive shaft, so measuring the torque of the drive shaft can effectively reflect the resistance during the entire trenching process.

The cutting resistance measurement scene is shown in Fig.4, mainly including a computer, universal testing machine, trenching blade, soil box, pressure head, resistance sensor (Range:0~30 kN, accuracy 1%), etc. Before the experiment, the soil moisture content was adjusted to 13.6%, and the compaction level was adjusted to 450 kPa (consistent with field conditions). The soil was filled into the soil box and compacted, excess soil was scraped off with a shovel. The universal testing machine was set to move at a speed of 250 mm/min. The trenching blade cut through the soil under the forced action of the pressure head (Fig.4b). The resistance sensor transmitted the measured cutting resistance to the computer in real time until the entire trenching blade was pressed into the soil, ending the test process. Then, it was adjusted to its original state, and CS blade was tested in the same manner.

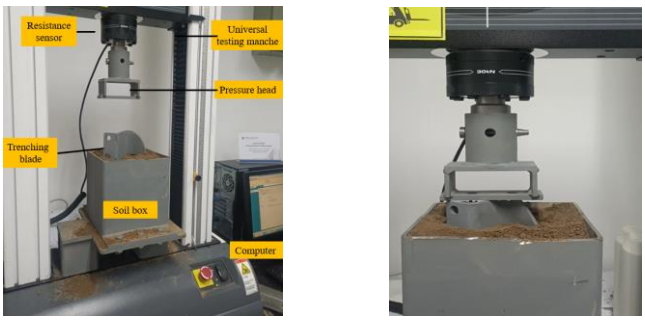

a) Experimental setup *b) Experimental process*

Fig. 4 - Single trenching blade test

To validate the optimization results, it is necessary to conduct on-site experiments to measure the mean trenching torque of the entire trenching system. The experiments are conducted at Yifeng Machinery Co., Ltd. in Gaomi City, Shandong Province. The soil at the experimental site is the same as that of the vineyard soil. Before the experiment, soil density was measured using the ring knife method, which was approximately 1500 kg/m³. The soil moisture content was determined to be around 13.6% using a moisture meter (TDR150, American Spectrometer, accuracy 3%, resolution 0.1%). The soil compaction measured using the Soil Compaction Meter (SC900, American Spectrometer, maximum depth 45 cm) is between 400-500 kPa. To accurately obtain the torque, a torque sensor (HCNJ-101 type, Beijing Haibohua, range 0~800 Nm, accuracy 0.5%) was used as the information perception component (Fig. 5a). The tractor provides power for the trenching device, and under the drive of the trenching shaft, the torque sensor rotates synchronously, and the output electrical signal is converted into a voltage value through the F/V conversion module. The data acquisition card displays the voltage signal on the computer with a sampling frequency of 20 Hz. The specific torque value was then determined using a linear mapping relationship (Fig.5b).

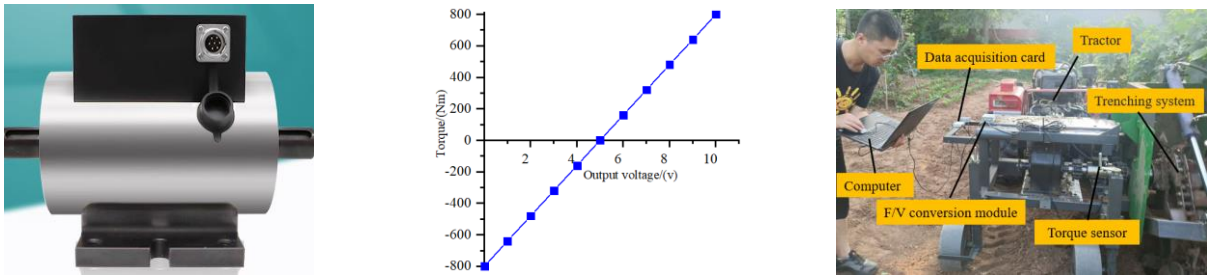

a) Torque sensor *b) The relationship between voltage and torque* *c) Mean torque measurement*

Fig. 5 - Field test

During the experiment, the CS blades were first tested, followed by testing the BS blades on the same land while maintaining the same operating parameters (Fig. 5c). Data analysis was performed during the stable working stage in the middle. The experiment was conducted three times, and the average value was selected as the final value.

RESULTS

Optimization and simulation analysis were conducted on the structural parameters of the trenching blades in order to obtain the variance analysis results for cutting resistance, as shown in Table 3. Based on the variance results, regression fitting was performed on the response variables, leading to the regression equations shown in Eq. (5).

Table 3

Analysis of variance for maximum cutting force

Dependent variable	Source of variance	Sum of square	Degree of freedom	*F* value	*P* value
F_1	β	47915.73	1	41.72	<0.0001**
	α	242800	1	211.39	<0.0001**
	R	54898.32	1	47.80	<0.0001**
	θ	93793.76	1	81.67	<0.0001**
	$\beta\alpha$	2679.87	1	2.33	0.1450
	βR	11031.83	1	9.61	0.0065**
	$\beta\theta$	899.55	1	0.78	0.3885
	αR	12696.22	1	11.06	0.0040**
	$\alpha\theta$	1858.69	1	1.62	0.2204
	$R\theta$	7892.99	1	6.87	0.0179**
	β^2	9504.22	1	8.28	0.0105**
	R^2	53.15	1	0.046	0.8322

Note：** represents factor with a highly significant influence on the index (P < 0.05)

$$F_1 = 768.83 + 44.68\beta + 100.57\alpha + 47.83R - 62.51\theta - 12.94\beta\alpha + 26.26\beta R + 7.5\beta\theta + 28.17\alpha R - 10.78\alpha\theta - 22.21R\theta - 18.43\beta^2 - 6.24R^2 \quad (5)$$

From the variance analysis results in the table, it can be noted that the factors α, β, R, and θ all have a significant impact on the maximum cutting force (F_1). Additionally, the interactions between the radius (R) and bending line angle (α), the radius R and the cone residual angle (θ), as well as the radius (R) and curvature (β), have a significant influence on F_1.

Single Factor Analysis

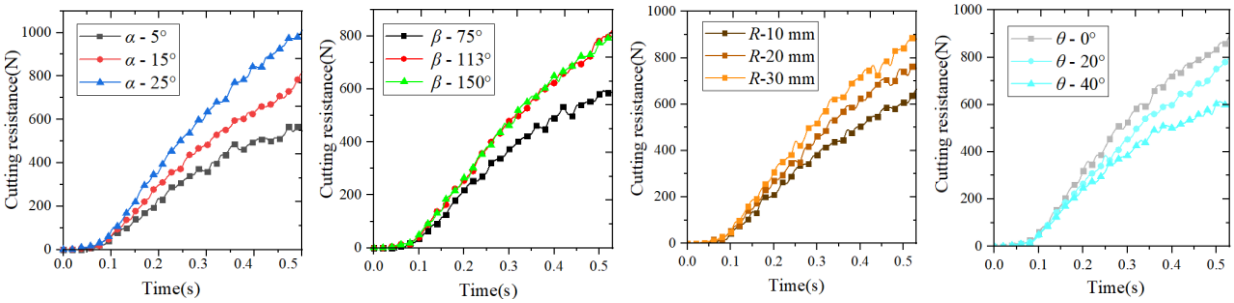

a) Bending line angle α *b) Curvature β* *c) Bend radius R* *d) Cone residual angle θ*

Fig. 6 - Single factor analysis

Keep three factors at middle levels, and the remaining factors at low, medium, and high levels respectively. Analyze the influence of each structural parameter on the cutting resistance. As illustrated in Fig. 6(a)~(c), during the initial 0.07 seconds, the trenching blade did not penetrate the soil, resulting in zero cutting resistance. From 0.07 to 0.55 seconds, the cutting resistance gradually increased and reached its maximum at the final moment. As demonstrated in Fig(a)~(c), the bending line angle α and radius R showed a positive correlation with cutting resistance; with the increase in α and R, the cutting resistance on the trenching blade increased, peaking when α was 25°and R was 30 mm. Analysis from Fig(b) indicated that the cutting resistance was minimum at 588 N when angle β was 75°. Although the resistance increased for β at 113° and 150°, the relationship weakened, indicating that the resistance did not increase linearly with β. Conversely, the cone residual angle θ had a negative correlation with cutting resistance; when θ was at its maximum, the cutting resistance was at its minimum. This is because θ directly determines the size of the cutting surface; a larger θ results in a smaller cutting surface, reducing the interaction area with the soil and thus decreasing the force, which aligns with the results of the mechanical analysis.

Interaction Analysis

The significant interaction terms are analyzed. From fig. 7(a)~(c), it can be noticed that regardless of the levels of β, α, and θ, F_1 gradually increases with an increase in R. When β and α are at a higher level, the increase in F_1 is much greater compared to when they are at a lower level (Fig.7(a) and (b)). Conversely, when θ is at a higher level, the increase in F_1 is lower compared to when it is at a lower level. Similarly, regardless of the radius level, the changes in F_1 are positively correlated with α and β and negatively correlated with θ, consistent with the findings of the single-factor analysis of F_1. Additionally, it was found that reducing α is easier in lowering F_1 compared to reducing β or increasing θ. Hence, to achieve a lower F_1, it is preferable to choose smaller values of α and β and a larger value of θ.

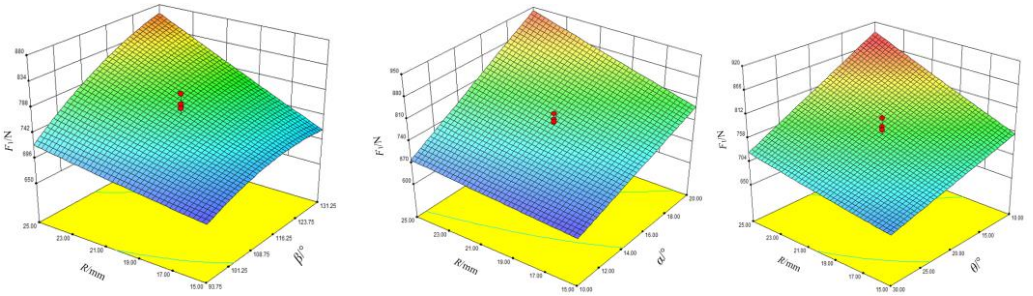

a) The impact of R and β on F_1 *b) The impact of R and β on F_1* *c) The impact of R and β on F_1*

Fig. 7 - Response surfaces of F_1

Parameter Optimization and Experimental Verification

Considering the interaction among different factors and in order to obtain the optimal combination of trenching blade structural parameters, the minimization of cutting resistance was adopted as the optimization criterion to determine the parameter values of each factor. The calculation objective is as shown in formula (6).

$$\begin{cases} \min F_1 \\ 93.75^{\circ} \le \beta \le 131.75^{\circ} \\ 10^{\circ} \le \alpha \le 20^{\circ} \\ 15 \le R \le 25 \\ 0^{\circ} \le \theta \le 40^{\circ} \end{cases} \quad (6)$$

Through numerical optimization, the optimized values for the curvature (β), bending line angle (α), radius (R), and cone residual angle (θ) that minimize F_1 are found to be 95°, 10°, 24 mm, and 39° respectively. According to the solution parameters, the trenching blade is processed (BS blades), as shown in Fig. 8 in comparison with CS blades.

a) CS blades *b) BS blades*

Fig. 8 - Comparison between the CS and BS blades

The only difference between different models of trenching blades was the length of the extending surface, while the cutting surface was the same. The optimized parameters mentioned above belonged to the optimization of the cutting surface. Therefore, according to the method shown in Fig. 4, it was only necessary to select the same model of BS and CS trenching blades (model 25) for the physical experiment. The test results were shown in Fig. 9, which illustrates the forces acting on the trenching blades over time. From the graph, it can be seen that as time increased, the force on the trenching blades also gradually increased, and the force curves of the two types changed in a similar manner. The force change was relatively slow in the 5-12 second stage, and it sharply increased in the 12-20 second stage. The force curve of the BS blade was lower than that of the CS blade, indicating that the trenching blades processed according to the optimized parameters could reduce the cutting resistance. The force on the BS blade peaked at 532.19 N, compared to 654.3 N for the CS blade, a reduction of 18.7%. This reduction indicates that the optimized trenching blade exhibits superior operational characteristics.

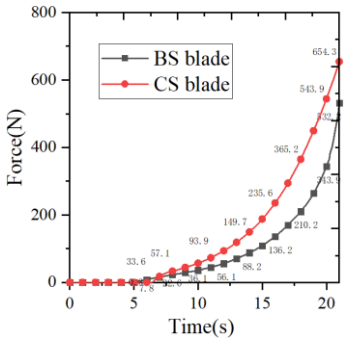

Fig. 9 - Results of soil cutting test

Field experiment

In LabVIEW (2018) software, a program was created and written through the graphical programming environment for cyclic acquisition of torque sensor signals. The CS and BS trenching blades were subsequently fixed to the chain trenching device using bolts, and field tests were conducted, with the test scene shown in Fig.10. The tractor output shaft speed is 540 r/min. For the convenience of data processing and analysis, the torque data from the middle 60 seconds was selected as a reference, dividing this 60-second period into six stages, each lasting 10 seconds. The average torque value for each stage was calculated within that stage, and the average values from these six stages were aggregated to serve as the final measurement result, as shown in Table 4.

a) Testing process *b) Effect chart after test*

Fig. 10 --Field experiment

According to Table 4, the average torque when using the CS trenching blade was 461.01 Nm, and when using the BS trenching blade, it was 416.66 Nm. Compared to CS blade, the mean torque was reduced by 9.62%. This indicates that the optimized trenching blade can significantly reduce the resistance of the entire trenching system and achieve excellent operational performance.

Table 4

Result of mean torque test

Type	Time/s						Mean torque/Nm
	0-10	10-20	20-30	30-40	40-50	50-60	
CS blades	470.60	471.14	445.02	448.98	491.43	441.14	461.01
BS blades	395.85	419.06	374.99	87.77	461.94	461.89	416.66

CONCLUSIONS

To address the issue of high tillage resistance during deep ditching, our study proposed a chain type reverse-rotary trenching device, and reached the following conclusions:

(1) A three-dimensional mathematical model for the trenching blade was established by transforming into the Cartesian coordinate system. Analyzing the structure of the trenching blade, the structural parameters affecting the efficiency of the trenching operation were identified as curvature, bending line inclination, bend radius, and cone residual angle.

(2) A simulation experiment was conducted with curvature, bending line inclination, bend radius, and cone residual angle as experimental factors, and soil cutting resistance as the index. Through single-factor and interaction analysis, the influence patterns of each factor on soil cutting resistance were determined. Employing a multi-objective optimization algorithm, the optimal parameter combination for the trenching blade was obtained as: β=95°, α=10°, R=24 mm, θ=39°.

(3) According to the optimal parameters, the trenching blades were processed and tested for validation. Measurements from a universal testing machine showed that the BS blades experienced less resistance than the CS blades, with a reduction of 18.7%. Field trenching test data indicated that the mean torque of the trenching device equipped with BS blades was 416.66 Nm, while that with CS blades was 461.01 Nm, which shows a decrease of 9.62%. This demonstrates that the trenching blades optimized through experimental testing can effectively reduce operational resistance and exhibit good operational performance.

ACKNOWLEDGEMENTS

This study was supported by Key Research and Development Program of Shandong Province (Science and Technology Innovation Boosting Action Plan for Rural Revitalization, Project Name: Research and Development of Intelligent Equipment for Grapes; Project Number: 2022TZXD001102-2), and China Agriculture Research System of MOF and MARA (CARS-29).

REFERENCES

[1] Azimi-Nejadian, H., Karparvarfard, S. H., & Naderi-Boldaji, M. (2022). Weed seed burial as affected by mouldboard design parameters, ploughing depth and speed: DEM simulations and experimental validation. *Biosystems Engineering*, vol. 216, pp.79-92, Iran.

[2] Green, L., Webb, E., Johnson, E., Wynn, S., & Bogen, C. (2023). Cost-effective approach to explore key impacts on the environment from agricultural tools to inform sustainability improvements: inversion tillage as a case study. *Environmental Sciences Europe*, vol.35, pp.79-94, Germany.

[3] Hu, Z.Y., Guo, Y.K., & Ming, Y. (2017). Finite element analysis of a chain-type orchard fertilizer

trenching machine's trenching blade (一种链式果园施肥开沟机开沟刀的有限元分析). *Jiangsu Agricultural Sciences*, vol. 45, pp. 231-237, Jiangsu/China.

[4] Kim, J., Kwon, O.S., Hai, N.L.D., & Ko, J.H. (2019). Study on the Design of an Underwater Chain Trencher via a Genetic Algorithm. *Journal of Marine Science and Engineering*, vol. 7, pp. 429, Korea.

[5] Li, J., Li, H., Chen, Y., Lin, P., Zhang, Q., Cheng, Y., Yang, Z., & Huang, G. (2023). Research on Ditching Mechanism of Self-Excited Vibration Ditching Machine. *Agronomy*, vol. 13, pp. 905, Guangdong / China.

[6] Liu, G., Yao, J., Chen, Z., Han, X., & Zou, M. (2023). Mesoscopic analysis of drag reduction performance of bionic furrow opener based on the discrete element method. *Plos One*, vol.18, pp. e293750, Jilin/China.

[7] Ma, T., Qi, B., Sun, X., Liu, Y., Ren, Y., Sun, J., Zhang, B., & Wu, Q. (2024). Design and experiment of self-propelled multifunctional trenching and fertilizing machine. *INMATEH Agricultural Engineering*. vol.74, pp.449-459, Bucharest / Romania.

[8] Sadek, M. A., Chen, Y., & Zeng, Z. (2021). Draft force prediction for a high-speed disc implement using discrete element modelling. *Biosystems Engineering*, vol. 202, pp. 133-141, Canada.

[9] Sitorus, P.E., Ko, J.H., & Kwon, O.S. (2016). Parameter study of chain trenching machines of Underwater Construction Robots via analytical model. In MTS/IEEE OCEANS 2016 Monterey, pp.1-6, Korea.

[10] Song, C., Zhang, X., Li, H., Lv, Y., Li, Y., Wang, X., Wei, Z., & Cheng, X. (2022). Effect of tine furrow opener on soil movement laws using the discrete element method and soil bin study. *INMATEH - Agricultural Engineering*, vol.68, pp.350-366, Bucharest / Romania.

[11] Song, Y., Xu, J., Xing, J., Wang, X., Hu, C., Wang, L., & Li, W. (2024). Research and Experiment on the Ditching Performance of a Ditching and Film-Covering Machine in the Yellow Sand Cultivation Mode of Solar Greenhouses. *Agronomy*, vol.14, pp.1704-1731, Xinjiang/China.

[12] Wang, J., Xu, Y., Wang, C., Xiang, Y., & Tang, H. (2023). Design and simulation of a trenching device for rice straw burial and trenching based on MBD-DEM. *Computers and Electronics in Agriculture*, vol.207, pp.107722, Harbin/China.

[13] Wang, L., Zhou, B., Wan, C., & Zhou, L. (2024). Structural parameter optimization of a furrow opener based on EDEM software. *International Journal of Agricultural and Biological Engineering*, vol.17, pp.115-120, Xinjiang/China.

[14] Wang, X., Zhang, S., Du, R., Zhou, H., & Ji, J. (2024). Recent Advances in Biomimetic Methods for Tillage Resistance Reduction in Agricultural Soil-Engaging Tools. *Agronomy*, vol. 14, pp. 2163, Henan/ China.

[15] Wei, L., Huang, W., Liu, J., Li, M., Zheng, Z., Wang, S., Du, D., & Zhang, Y. (2024). DEM simulation of subsoiling in tropical sugarcane fields: Effects of opposing subsoiler design and model parameters. *Smart Agricultural Technology*, vol.9, pp.100593, Guangdong/China.

[16] Zeng, Y., Li, J., Li, H., Zhang, Q., Li, C., Li, Z., Jiang, R., Mai, C., Ma, Z., & He, H. (2024). Research on the ditching resistance reduction of self-excited vibrations ditching device based on MBD-DEM coupling simulation. *Frontiers in Plant Science*, vol.15, Guangdong/China.

[17] Zhang, X., Zhang, L., Hu, X., Wang, H., Shi, X., & Ma, X. (2022). Simulation of Soil Cutting and Power Consumption Optimization of a Typical Rotary Tillage Soil Blade. *Applied Sciences*, vol.12, pp.8177, Xinjiang/China.